



**HAL**  
open science

## Experiments and nonlinear simulations of a rubber isolator subjected to harmonic and random vibrations

T Roncen, Jean-Jacques Sinou, J-P Lambelin

► **To cite this version:**

T Roncen, Jean-Jacques Sinou, J-P Lambelin. Experiments and nonlinear simulations of a rubber isolator subjected to harmonic and random vibrations. *Journal of Sound and Vibration*, 2019, 451, pp.71 - 83. 10.1016/j.jsv.2019.03.017 . hal-03255533

**HAL Id: hal-03255533**

**<https://hal.science/hal-03255533>**

Submitted on 9 Jun 2021

**HAL** is a multi-disciplinary open access archive for the deposit and dissemination of scientific research documents, whether they are published or not. The documents may come from teaching and research institutions in France or abroad, or from public or private research centers.

L'archive ouverte pluridisciplinaire **HAL**, est destinée au dépôt et à la diffusion de documents scientifiques de niveau recherche, publiés ou non, émanant des établissements d'enseignement et de recherche français ou étrangers, des laboratoires publics ou privés.

# Experiments and nonlinear simulations of a rubber isolator subjected to harmonic and random vibrations

T. Roncen<sup>a,b</sup>, J-J. Sinou<sup>b,c</sup> and J-P. Lambelin<sup>a</sup>

<sup>a</sup> CEA, DAM, CESTA, F-33114 Le Barp, France

<sup>b</sup> Laboratoire de Tribologie et Dynamique des Systèmes UMR CNRS 5513, Ecole Centrale de Lyon, France

<sup>c</sup> Institut Universitaire de France, 75005 Paris, France

---

## Abstract

This paper presents experiments and numerical simulations of a nonlinear rubber isolator subjected to both harmonic and broadband random excitations. Harmonic and broadband random excitations are performed experimentally in order to show the softening effect of the rubber isolator for high amplitudes of displacement and to show the temperature dependency of its mechanical properties. Firstly, the rubber isolator is modeled as a one degree-of-freedom system, whose stiffness and damping depend only on the amplitude of the relative displacement of the joint. The relationship between the stiffness and the damping versus the amplitude of the relative displacement of the rubber isolator is updated via experiments. Secondly, the Harmonic Balance Method (HBM) and the shooting method are presented and extended to take into account both harmonic and random excitations. A modification of the nonlinear methods is necessary in order to recover the information concerning the displacement amplitude. Moreover, for random excitations, a periodogram strategy is used to ensure a good estimate of the resulting Power Spectral Density (PSD). Finally, comparisons between experiments and simulations are undertaken. Good correlations are observed for harmonic and broadband random excitations, thus validating the modeling of the rubber isolator and the proposed nonlinear methodology.

---

## 1. Introduction

Elastomers have received considerable attention in recent years due to their applicability in numerous engineering areas, including space applications, actuators, sensors, robotics, bio-engineering devices and civil engineering structures. Their wide use in industry is due to their relative softness and their capability to withstand deformation of up to several hundred percent while resuming their original shape after stress release. Knowledge of rubber material properties is essential when rubber compounds are included in dynamic systems. However this knowledge is often rather poor due to the complex behavior of rubber materials, with mechanical properties such as dynamic hardness and damping that are dependent not only on the fillers in the material but also on temperature and the frequency and amplitude of the motion. Nonlinearities in an elastomeric joint, due to either material properties or geometric influences, are often present as discussed by Harris and Stevenson [1]. Explanations on the underlying physical mechanisms of the nonlinearities are provided in [2].

The joint under study is a vibration isolator with nonlinear behavior, exhibiting dependency of eigenfrequencies and dissipation with input amplitude and temperature, hysteresis in the frequency response and multi-harmonic response to a mono-harmonic excitation. Many methods have been developed in the literature to study the dynamic behavior of filled rubber isolators. Firstly, these include methods based on the modeling of the mechanical laws of the elastomer, using physical models such as the Kelvin-Voigt or Maxwell model [3], fractional derivatives [4] or the Berg model [5] to name just a few. These methods are usually precise but require complex modeling of the joint, generally using a finite element discretization of the joint element [6, 7]. The second class of methods is based on phenomenological modeling integrated at the scale of the mechanism. They usually take

the form of a one degree-of-freedom system, the stiffness and damping of which are polynomials [8] or exponentials [9] of the relative displacement of the mechanism.

The approach used in the present work is based on this second class of modeling (i.e. phenomenological modeling of the joint), as the whole joint is modeled by a one degree-of-freedom mechanism. The uniaxial behavior of the joint is identified using swept-sine experiments with increasing level of excitation. The nature of the experiments hinders the recovery of the relation between the stiffness and damping with the relative displacement of the mechanism. Instead, the relation between the stiffness and damping with the amplitude of the relative displacement of the mechanism is obtainable. In structural dynamics, most nonlinear formulations express dependencies between the stiffness and damping with the relative displacement or derivatives of the relative displacement. Consequently, the stiffness and damping evolve at each instant according to the instantaneous values of the relative displacement or its derivatives. In this application though, the stiffness and damping evolve according to the amplitude of the relative displacement, which is no longer an instantaneous value. The main contribution of this present study is the extension of existing nonlinear methodologies in order to cope with this new formulation. The difficulty lies in the fact to be able to retrieve in the simulations information concerning the relative displacement amplitude at all times. To do so, a second time scale is introduced to solve the nonlinear problem during the simulation process.

Various simulation methods have been developed to compute a nonlinear frequency response function. Among them, the shooting method and the Harmonic Balance Method (HBM) are the most common, with academic problems [10] or industrial applications [11]. They are based on a periodic representation of the signal, along with a continuation method to obtain a continuous response curve. Both methods have been proven to work for harmonic excitations, and more recently for random excitations as well [12], with nonlinearities expressed as a function of time, such as the relative displacement.

This paper is divided into four parts. Firstly, a brief description of the test structure and the analysis of various experimental data from vibrational tests are presented. Secondly, the paper focuses on the modeling of the joint and the modeling of the signal depending on the type of excitation. Thirdly, the Harmonic Balance Method (HBM) and the shooting method are developed and extended in order to retrieve information on the relative displacement amplitude, which is necessary in order to compute the nonlinear simulation for both harmonic and random excitations. Last but not least, the simulations are validated for both types of excitation by comparison with the experiments.

## 2. Experiments

### 2.1. Experimental setup

The structure studied, named “Unitarian Gamma Joint”, is presented in Figure 1. The system consists of a vibration-absorbing elastomeric material of biconical shape, surrounded by an aluminum cage. In this paper, the whole assembly is referred to as a rubber isolator. The latter is fixed on a solid casing and linked to an axisymmetric flyweight of 0.625 kg. The solid casing is bolted to a shaker. The structure is designed to have one axial mode, stressing the elastomeric part of the joint, and initiating complex phenomena inside the material. The rotation center of the flyweight matches the rotation center of the elastomeric joint, in order to minimize the effect of tilting.

Two accelerometers ( $A1$  and  $A2$ ) are positioned on the top of the flyweight, at 180 degrees from each other, and one accelerometer is placed on the casing ( $P1$ ). Each signal is denoted by the sensor name followed by the direction of measurement. Adding the accelerometers on the flyweight lowers its rotation center by a very small value. The effect on the potential tilting of the joint element is negligible. The input signal  $P1Z$  is the shaker’s feedback control signal. The reference frame of the study is the base of the casing, where  $P1$  is fixed. The response signal is the acceleration at the top of the flyweight, in the reference frame of the casing, that is  $A1Z$  or  $A2Z$ . The signals  $A1Z$  and  $A2Z$  help us to check on the symmetry of the output signal and the absence of tilting in the response in the case of vertical input. Last but not least, a temperature sensor was positioned on top of the rubber isolator, in order to record any increase in the elastomer temperature.

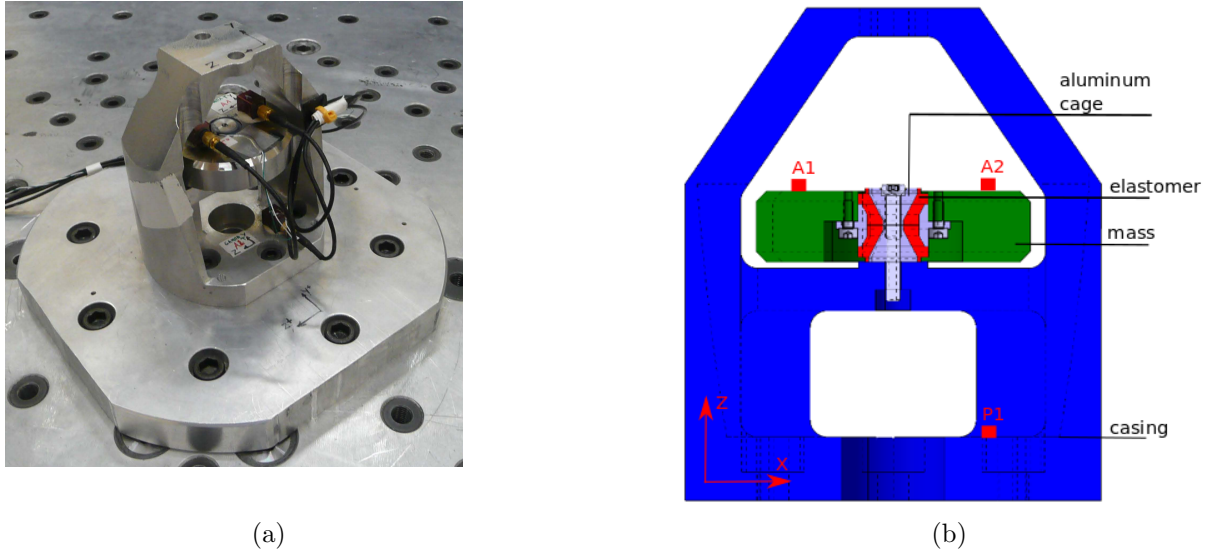


Figure 1: Experimental setup including 3 accelerometers ( $P1, A1, A2$ ) - (a) photo of the structure “Unitarian Gamma Joint” (b) schematic drawing with sensor positioning

## 2.2. Experimental results

Experiments are conducted in order to investigate the nonlinear response of the system under study and more precisely the dependency of the structural response with respect to excitation and temperature. It can be noted that the elastomer inside the joint corresponds to the main contribution for these nonlinear behaviors.

First, a set of experiments (both swept-sine excitations and random excitations) are conducted with an increasing level of excitation in order to observe the dependency of the response with respect to the deformation of the elastomer (Payne effect). The swept-sine experiments were conducted with input accelerations of [1; 2; 3; 4; 5; 6; 7; 8; 9; 10; 15; 20; 30; 40; 60; 80; 100; 120; 140; 160; 180; 200]  $\text{m s}^{-2}$ , while the random experiments were conducted with constant Power Spectral Density of [1; 20; 40; 80]  $(\text{m s}^{-2})^2/\text{Hz}$  over the frequency range [50;600] Hz. Figure 2 shows the evolution of the frequency response functions (FRF) for both the swept-sine experiments (Figure 2a) and the random excitations (Figure 2b). The FRF plots the ratio of the output acceleration over the input acceleration (i.e.  $A1Z/P1Z$ ). For a linear system, the FRF would have been unique for all the excitation levels. For the structure “Unitarian Gamma Joint”, a decrease in the resonance frequency is observed when the input excitation increases, from 430 Hz to 250 Hz for the swept-sine experiments. It corresponds to the softening of the elastomer when subjected to higher deformations (Payne effect). The vibration-damping role of the elastomer is also exacerbated for high excitation levels, as the resonance peak decreases when the input excitation increases. The same nonlinear phenomena appear for random excitations, with a shift in frequency from 430 Hz to 300 Hz and an increase in damping. For both types of excitation, an increase in the elastomer temperature was recorded for high excitation levels. The temperature rise is quite significant for high levels of excitation: +40 °C for the swept-sine experiment at 200  $(\text{m s}^{-2})^2/\text{Hz}$ , +5 °C for the random experiment at 80  $(\text{m s}^{-2})^2/\text{Hz}$ . The difference being that, for random excitations, the temperature is constant for the experiments whereas it varies considerably during the swept-sine experiments, depending on the swept-sine frequency.

Secondly, swept-sine experiments of equal input acceleration ( $1 \text{ m s}^{-2}$ ) were performed at different ambient temperatures. Figure 3a shows the evolution of the FRFs with respect to temperature. A decrease in the resonance frequency is observed when the ambient temperature increases, from 500 Hz at 0 °C to 370 Hz at 50 °C. This softening of an elastomer with respect to temperature is a common property of elastomers, well documented in the literature. It is notable that the resonance peak level is weakly affected by ambient temperature.

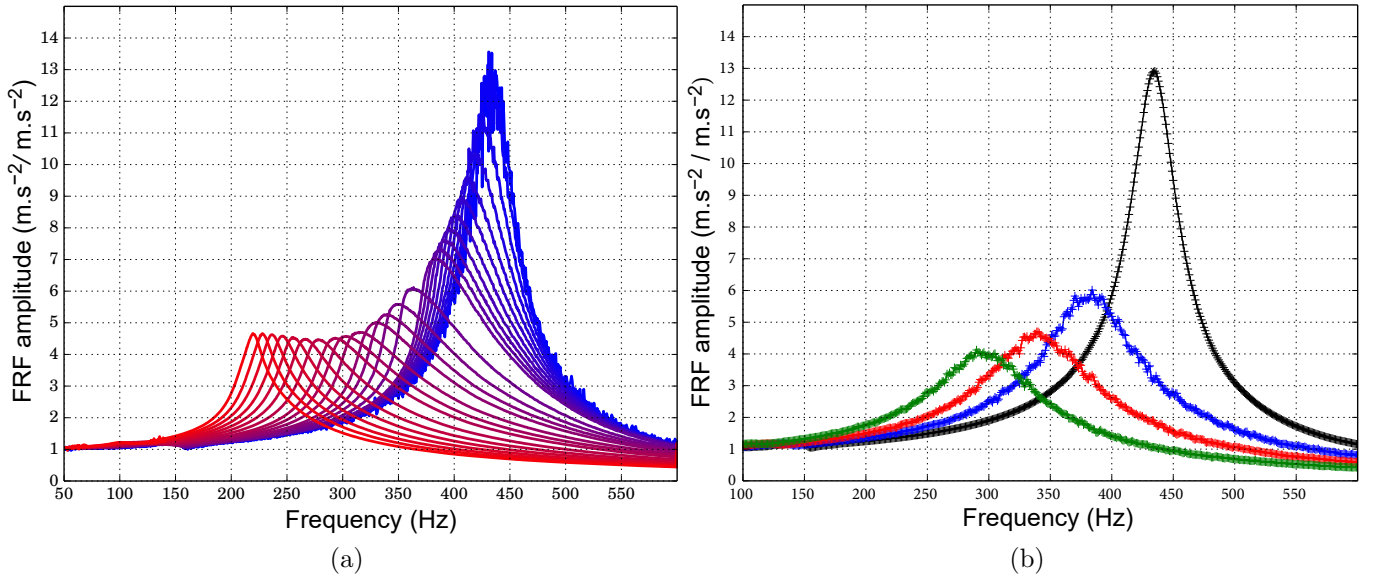


Figure 2: Experimental FRFs for (a) swept-sine experiments of excitation levels  $1\text{ m s}^{-2}$  (blue) to  $200\text{ m s}^{-2}$  (red) and (b) random signals of excitation levels with a constant RMS of  $1\text{ m s}^{-2}$  (black),  $20\text{ m s}^{-2}$  (blue),  $40\text{ m s}^{-2}$  (red),  $80\text{ m s}^{-2}$  (green)

Then, a series of swept-sine experiments are conducted repeatedly at  $1\text{ m s}^{-2}$  (blue curves) and  $100\text{ m s}^{-2}$  (red curves), as illustrated in Figure 3b. It is notable that, at first, for a given input acceleration, the frequency peak slowly goes towards lower resonance frequencies. Then a stabilization of the resonance peak is observed with a convergence to a fixed value. This behavior corresponds to the Mullins effect, where the stress-strain curve of the elastomer (i.e. its stiffness) depends on the maximum loading previously encountered. By alternating low and high levels of excitation, the elastomer's response converges to a unique FRF amplitude curve. Therefore, the reproducibility of the elastomer can be predicted. In conclusion, to ensure a quasi-perfect reproducibility of a given elastomer behavior at lower regimes, one has to take into account the potential Mullins effect and so to preliminary charge the elastomer at the highest desirable excitation (i.e.  $200\text{ m s}^{-2}$  in this study).

### 3. Modeling

In this section, the modeling of the elastomer as well as the validity of this chosen simplified modeling for the present study are first discussed. Secondly, a choice of signal modeling for easy use in the context of the non-linear simulations that will follow in Section 4 is then proposed. The modeling of both swept-sine experiments and random excitations will be discussed.

#### 3.1. Modeling of the structure “Unitarian Gamma Joint”

The present study is limited to the tension-compression of the elastomer joint. The experimental assembly is modeled by a one degree-of-freedom system. This model is independent of the type of excitation and therefore it will be used both for the case of swept-sine or random excitations.

A schematic diagram of the system “Unitarian Gamma Joint” is shown in Figure 4.  $M$  denotes the mass of the mechanical system. By neglecting the mass of the accelerometers positioned on the flyweight,  $M$  is equal to the flyweight's mass (i.e.  $M = 0.625\text{ kg}$ ).  $K$  and  $C$  define respectively the stiffness and the damping of the rubber isolator that depend on the amplitude of the relative displacement.  $X$  defines the relative displacement of the mass  $M$  and  $\hat{X}$  corresponds to the amplitude of  $X$ . In the present study it is assumed for the sake of simplicity that the stiffness  $K$  and the damping  $C$  are functions of only  $\hat{X}$ . These determinations of  $K(\hat{X})$  and  $C(\hat{X})$  will be proposed later in this section.

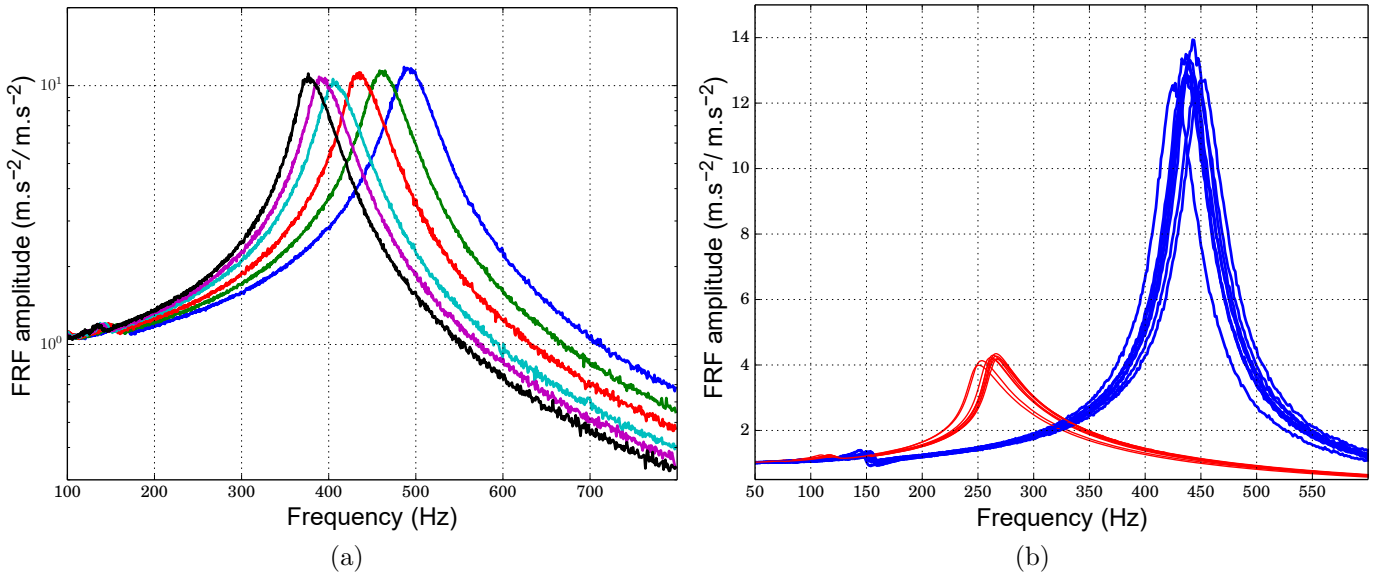


Figure 3: Experimentation on the notions of repeatability (a) Experimental FRFs for swept-sine experiments (a) of excitation levels  $1\text{m s}^{-2}$  with an ambient temperature of  $0\text{ }^{\circ}\text{C}$  (black),  $10\text{ }^{\circ}\text{C}$  (magenta),  $20\text{ }^{\circ}\text{C}$  (cyan),  $30\text{ }^{\circ}\text{C}$  (red),  $40\text{ }^{\circ}\text{C}$  (green) and  $50\text{ }^{\circ}\text{C}$  (blue) - (b) Experimental FRFs for swept-sine experiments of excitation levels  $1\text{m s}^{-2}$  (blue) and  $100\text{m s}^{-2}$  (red)

The shaker is piloted with an input acceleration, so the dynamic equation associated with the problem is written:

$$M\ddot{X}(t) + C(\hat{X})\dot{X}(t) + K(\hat{X})X(t) = -M\ddot{a}(t) \quad (1)$$

with  $a$  the input displacement at the base as illustrated in Figure 4. Equation (1) can be rewritten in the following form

$$\ddot{X} + 2\omega_0\xi\dot{X} + \omega_0^2X = -\ddot{a} \quad (2)$$

where  $\omega_0 = \sqrt{\frac{K}{M}}$  and  $\xi = \frac{C}{2M\omega_0}$  define the classical undamped angular frequency of the oscillator and the damping ratio. In the present case, it can be noted that these two quantities are dependent of  $\hat{X}$ . This dependency is not written explicitly to facilitate the reading of equations to the reader.

From a practical point of view, the experimental data are expressed in output displacement  $Y(t)$ , as indicated in Figure 4. So by considering the linear relation the output displacement  $Y(t)$  and the relative displacement  $X(t)$  (i.e.  $Y(t) = X(t) + a(t)$ ), Equation (2) can be rewritten by using the output experimental variable  $Y(t)$  such as

$$\ddot{Y} + 2\omega_0\xi\dot{Y} + \omega_0^2Y = \omega_0^2a + 2\omega_0\xi\dot{a} \quad (3)$$

The related transmissibility is given by

$$T(\omega) = \frac{1 + 2i\frac{\omega}{\omega_0}\xi}{1 - (\frac{\omega}{\omega_0})^2 + 2i\frac{\omega}{\omega_0}\xi} \quad (4)$$

By considering the previous relation 4, it may be noted that the maximum of the transmissibility is given by  $\|T(\omega)\|_{max} \approx \frac{1}{2\xi} = Q$ . This corresponds to the maximum of the resonance peak which is dependent of  $\hat{X}$  in the present case. This maximum  $\|T(\omega)\|_{max}$  is obtained for  $\omega_{max} = \omega_0\sqrt{1 - 2\xi^2}$ .

The experimental process to identify the unknown functions  $C(\hat{X})$  and  $K(\hat{X})$  will now be explained. This process is based on the use of swept-sine experiments for different acceleration levels  $\ddot{a}$ . For a given acceleration level  $\ddot{a}$ , a swept-sine experiment for which frequency evolves slowly enough (i.e. 1 octave/min in the vicinity of the resonance) is performed. For the reader

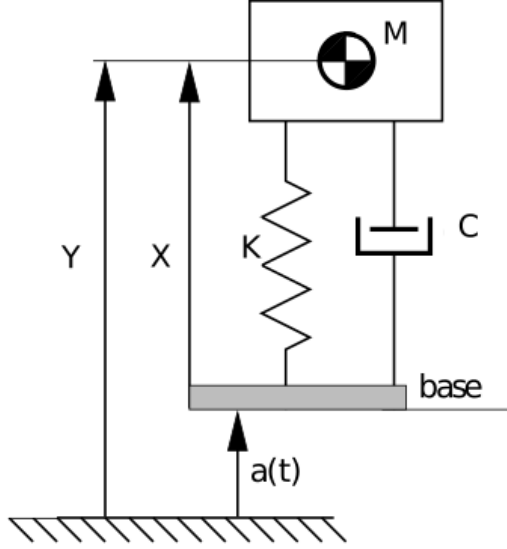


Figure 4: Diagram of the rubber isolator modeled by a spring mass system

comprehension, the use of a slow evolution of the frequency allows to consider that the response  $X$  can be estimated as being stationary over a short time. In other words the response  $X(t)$  can be approximated by its fundamental for all the swept-sine experiment by considering the following relation

$$X(t) = \hat{X}(\omega) \sin(\omega t) \quad (5)$$

This formulation allows to define the displacement amplitude  $\hat{X}(\omega)$  as a function of the experimental frequency for a given acceleration level  $\ddot{a}$ . Thus, for one swept-sine experiment at a given acceleration level  $\ddot{a}$ , it is easily possible to identify the following experimental values: the maximum amplitude  $\hat{X}_{max}$ , the associated angular frequency  $\omega_{max}$  and the associated quality factor  $Q$ . The experimental identification of these three quantities makes it possible to estimate the equivalent damping ratio  $\xi = \frac{1}{2Q}$  and the equivalent undamped angular frequency of the oscillator  $\omega_0 = \frac{\omega_{max}}{\sqrt{1 - 2\xi^2}}$ . Finally

the unknown values of the stiffness  $K$  and the damping  $C$  of the rubber isolator can be deduced from  $\xi$  and  $\omega_0$ . It is brought to the attention of the reader that the two values of  $\xi$  and  $\omega_0$  as well as  $K$  and  $C$  are calculated, and therefore theoretically valid, only for the relative displacement  $\hat{X}_{max}$ .

Then repeating the same procedure for various acceleration levels, it is possible to find experimentally the functions of dependencies of the equivalent damping ratio  $\xi$  and the equivalent undamped angular frequency of the oscillator  $\omega_0$  as well as the stiffness  $K$  and the damping  $C$  of the rubber isolator versus the maximum displacement amplitude  $\hat{X}_{max}$ . Figure 5 shows the experimental identification of the stiffness and the damping of the rubber isolator by using this proposed procedure: each point corresponds to one swept-sine experiment at a given acceleration level and the calculation of the associated quality factor  $Q$ , the equivalent damping ratio  $\xi$  and the equivalent undamped angular frequency  $\omega_0$  at the maximum amplitude  $\hat{X}_{max}$ , which leads to the estimation of  $K$  and  $C$ . Using a spline interpolation, the stiffness  $K$  and damping  $C$  of the elastomer joint are defined as continuous functions of  $\hat{X}_{max}$ . Finally, it is recalled that the functions obtained are established only at the peak of resonance, in other words only according to the variable  $\hat{X}_{max}$ . In the remainder of the study, it is admitted that the stiffness  $K$  and damping  $C$  are only dependent on the amplitude of displacement  $\hat{X}$ . Therefore it will be assumed that these identified values of  $K$  and  $C$  as a function of the amplitude of displacement are valid whatever the frequency considered. This decisive choice for the remainder of the study is explained by the desire to propose a simplified modeling of the elastomer via a reduce number of simple dedicated experiments. This modeling and its associated limitation for the prediction of the nonlinear response have now to be tested by performing comparisons between experiments and simulations for the mechanical system subjected to random excitation. This will be the subject of Section 5.3.

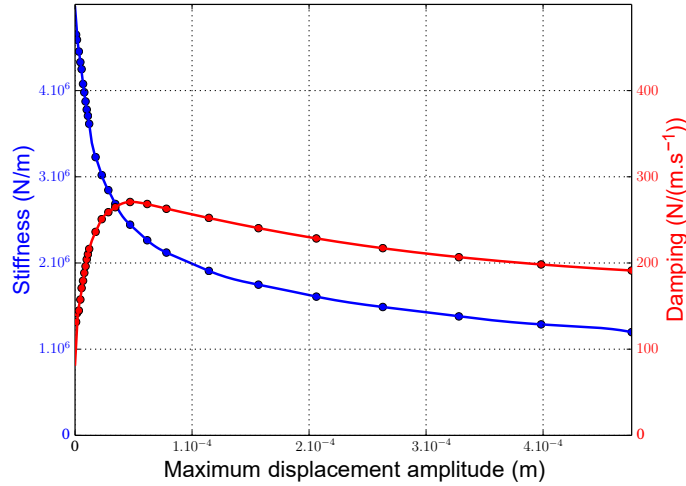


Figure 5: Evolution of the stiffness (blue) and the damping (red) with respect to the displacement amplitude

### 3.2. Discussion on the validity of the modeling from multi-harmonic experimental measurements

The aim of this section is to discuss the validity of the previous simplified modeling choice of the elastomer regarding the multi-harmonic response measurements observed via experiments.

indeed, considering the experimental protocol, the vibrator is piloted with a logarithmic swept sine signal. The frequency evolves slowly enough (1 octave/min in the vicinity of the resonance) to consider the response to be stationary. In the vicinity of each time point, both input and output signals are periodic and can thus be developed in a Fourier series. The signal analysis tool developed in [10] aims at identifying at each instant the fundamental frequency and the harmonics amplitudes of both input and output signals. This identification is treated as a nonlinear optimization problem. The parameters are evaluated, bounded and then optimized using the Covariance Matrix Adaptation and Evolution Strategy (CMAES) [13] which is an evolutionary algorithm chosen because of its quick convergence and its low noise sensitivity.

The experimental harmonic curves of the input and output are plotted in Figure 6 for an acceleration input of  $40 \text{ m s}^{-2}$ . The harmonic components of orders 2 and 3 are visible on the experimental response of the mechanical system. It is also clearly shown that the experimental input contains  $2\times$  and  $3\times$  harmonic components. As previously discussed in Section 3.1, the simplified modeling of the elastomer links together the stiffness and the damping of the system to a displacement amplitude. This amplitude is calculated under the hypothesis that the response can be approximated by its fundamental, as indicated in Equation (5). Due to the fact that the experimental results given in Figure 6 show the presence of nonlinear contributions of orders 2 and 3 on both the output response and the input excitation, the validity of this hypothesis has to be investigated. However, since the harmonic acceleration outputs are rather small compared to the fundamental acceleration of the response (ratio less than 2 percent for the second harmonic and less than 0.2 percent for the third harmonic), it is assumed that the main nonlinear phenomenon at stake is the Payne effect, which is a dependency of the response to the displacement amplitude. The higher harmonics make a very small contribution to the global displacement and hence can be neglected for the remainder of the study, which validates the simplified formulation used in the previous section.

### 3.3. Modeling of the signal

As previously shown in Section 2, swept-sine experiments and random excitations are performed independently on the system “Unitarian Gamma Joint” under study. Each excitation has to be modeled for the forthcoming nonlinear simulations. The two methods that will be implemented to predict the nonlinear responses are the shooting method and the HBM (see details in Section 4). The inputs for the shooting method (the HBM, respectively) are periodic temporal signals (a Fourier transform of the input signal, respectively). The remainder of this section briefly describes the modeling chosen for the modeling of a swept-sine temporal or random signal.

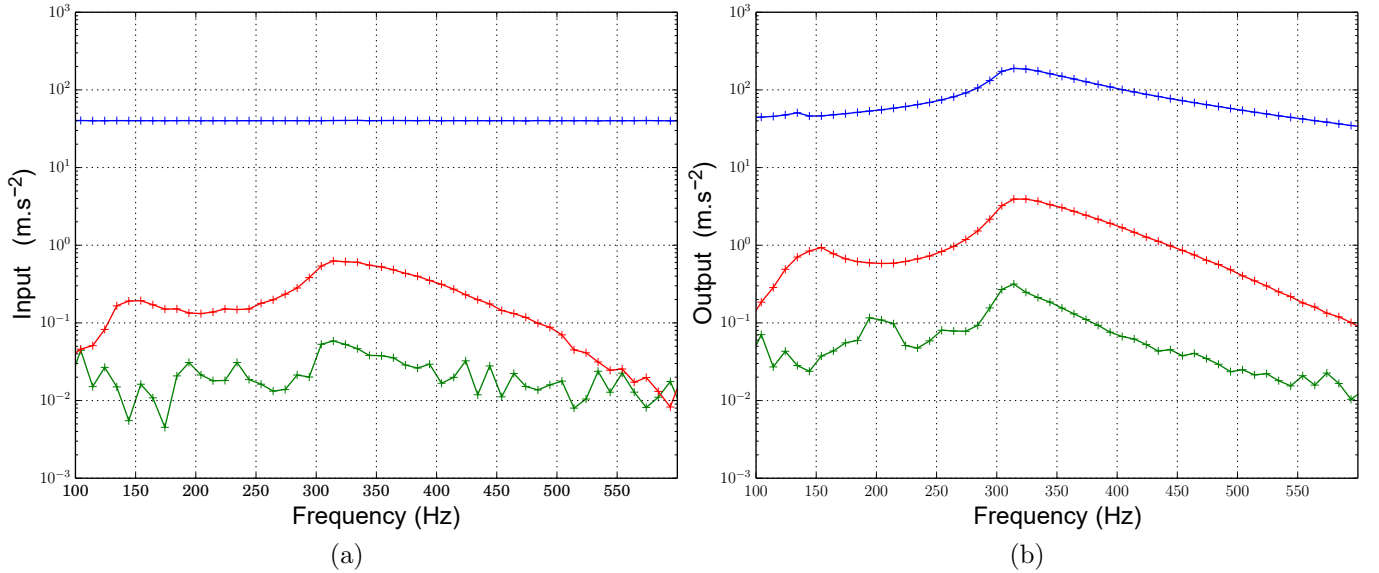


Figure 6: Input (a) and output (b) experimental harmonics for the experiment with a constant excitation level of  $40 \text{ m s}^{-2}$  for harmonics 1 (blue), 2 (green) and 3 (red)

### 3.3.1. Modeling of a swept-sine temporal signal

For a given pulse  $\omega$ , the swept-sine temporal signal is modeled by a mono-harmonic source term with constant acceleration amplitude:

$$\ddot{a} = A(\omega) \sin(\omega t) \quad \forall t \quad \text{and} \quad A(\omega) = A_0 \quad \forall \omega \quad (6)$$

with  $a$  the displacement at the base. This signal is periodic and therefore eligible for the two nonlinear methods (i.e. the shooting method and the Harmonic Balance Method) used in the present study.

### 3.3.2. Modeling of a random signal

The modeling of random excitations based on trigonometrical series to describe a random signal [14, 15] is now briefly described and detailed. More details can be found in [12].

Let  $x(t)$  be a second order, stationary, centered and Gaussian process.  $x(t)$  is assumed to have a Power Spectral Density  $S_x(f)$ , with a compact support, meaning that there is a frequency  $f_m > 0$  for which  $S_x(f) = 0$  for  $\|f\| > f_m$ . A discretization on the compact interval  $[-f_m, +f_m]$  is chosen. Let  $dt$  be the time interval  $dt$  defined by  $dt = \frac{1}{f_c}$  where  $f_c$  corresponds to the Nyquist-frequency  $f_c$  that must be at least twice the maximum frequency observed in the study (i.e.  $f_c > 2f_m$ ). Let  $N$  be a fixed integer (of power of 2). By considering  $\Delta f = \frac{f_c}{N}$ , a family of frequencies adapted to FFT [16] is defined as follows

$$f = \left[ 0, \frac{1}{Ndt}, \frac{2}{Ndt}, \dots, \frac{f_c}{2}, -\frac{f_c - 1/dt}{2}, -\frac{f_c - 2/dt}{2}, \dots, -\frac{1}{Ndt} \right] \quad (7)$$

To simulate a signal  $x(t)$ , a series of processes  $x^N(t)$  converging toward  $x(t)$  is used. According to Shinozuka [15],  $x^N(t)$  can be defined as follows

$$x^N(t) = \sqrt{\frac{1}{T}} \sum_{k=0}^{N-1} \sqrt{S_x(f_k)} \cos(2\pi f_k t + \Phi_k) \quad (8)$$

where  $S_x(f)$  defines the knowledge of the PSD of the signal  $x(t)$ . This series of cosines contains equidistributed frequencies on the interval  $[-\frac{f_c}{2}, +\frac{f_c}{2}]$  with random phases uniformly distributed on  $[0, 2\pi]$  and with an amplitude function of  $S_x(f)$ .  $\Phi$  is a family of random phases uniformly distributed on  $[0, 2\pi]$  that is organized in a similar way to Equation (7)

$$\Phi = [\Phi_0, \Phi_1, \Phi_2, \dots, \Phi_{(N-1)/2}, -\Phi_{(N-3)/2}, -\Phi_{(N-5)/2}, \dots, -\Phi_2, -\Phi_1] \quad (9)$$

It can be noted that this series is constrained by the relation  $\Phi_{f_k} = -\Phi_{-f_k}$  due to the fact that the output signal will only have real values.

Due to the fact that the computational time of the series (8) can be prohibitive for very high value of  $N$  (i.e. large samples) Equation (8) can be rewritten in the following form:

$$x^N(t_n) = \sqrt{\frac{1}{T}} \text{Re} \left( \text{FFT}^{-1} (e^{i\Phi_k} \sqrt{S_x[f_k]}) \right) \quad (10)$$

This new formulation corresponds to the previous form (8) for times  $t$  equidistant and with a frequency discretization chosen in order to use FFT algorithms.

More details on the use of this process in the numerical simulation methodology are available in [12].

## 4. Simulation

One of the main objective of this section is to explain the adaptations to be made on the two classical nonlinear methods, namely the shooting method and the HBM. First of all, it may be mentioned that these two nonlinear methods classically takes into account harmonic signals with deterministic responses. A generalization of these methods has been developed in [12] in order to take into account random signals as well. So a brief reminder is proposed in this section on the subject. Moreover the mandatory modification of the two nonlinear methods due to the modeling of the rubber isolator (i.e. the nonlinear dependency on the amplitude of the displacement) is discussed. In this section, the two nonlinear methods are presented under a general form that can be used for either harmonic or random signals. The differences in the methodology imputable to the source of excitation are highlighted.

### 4.1. Harmonic Balance Method

In this section, it is proposed to solve the nonlinear problem defined in Equation (1) by applying the Harmonic Balance Method [17]. The nonlinear problem is rewritten by splitting the constant parts  $C_{lin}$  and  $K_{lin}$  from the nonlinear parts  $C_{nl}$  and  $K_{nl}$  of the stiffness  $K(\hat{X})$  and the damping  $C(\hat{X})$  respectively:

$$M\ddot{X}(t) + C_{lin}\dot{X}(t) + K_{lin}X(t) = F(t) + F_{nl}(X) \quad (11)$$

with:

$$F_{nl}(X) = \left( C_{lin} - C_{nl}(\hat{X}) \right) \dot{X}(t) + \left( K_{lin} - K_{nl}(\hat{X}) \right) X(t) \quad (12)$$

$C_{lin}$  and  $K_{lin}$  corresponds to the experimental values calculated at the lowest excitation level, for which it is assumed that the stiffness  $K(\hat{X})$  and the damping  $C(\hat{X})$  can still be considered as linear functions versus the amplitude. Consequently  $C_{nl}(\hat{X})$  and  $K_{nl}(\hat{X})$  are the associated contributions to define the non-linear dependency of the stiffness  $K$  and the damping  $C$  with respect to the amplitude  $\hat{X}$ .

Let  $\Omega = 2\pi\Delta f$  be the fundamental pulsation. For swept-sine simulations,  $\Omega$  corresponds to the current pulsation of the excitation, while it corresponds to the frequency discretization for random excitations.

The stationary solution is assumed to be approximated by a truncated Fourier series with  $\Delta f$  as fundamental frequency such as

$$X(t) = B_0 + \sum_{k=1}^p (B_k \cos(k\Omega t) + A_k \sin(k\Omega t)) \quad (13)$$

where  $(B_0, (A_k, B_k)_{k \in [1;p]})$  are the Fourier coefficients of the solution  $X$ . Both the nonlinear dynamical response and the force vector are also approximated by a finite Fourier series

$$F_{nl}(t) = C_0 + \sum_{k=1}^p (C_k \cos(k\Omega t) + S_k \sin(k\Omega t)) \quad (14)$$

$$F(t) = \sum_{k=1}^p (C_{k,excit} \cos(k\Omega t) + S_{k,excit} \sin(k\Omega t)) \quad (15)$$

where  $(C_0, (S_k, C_k)_{k \in [1;p]})$  and  $(S_{k,excit}, C_{k,excit})_{k \in [1;p]}$  are respectively the Fourier coefficients of the nonlinear force  $F_{NL}$  and the excitation  $F$ . The order of the truncated Fourier series, denoted  $p$  in previous equations, is selected on the basis of the number of significant harmonics required in the dynamical response. For the case of swept-sine experiments, the hypothesis made in Section 3 limits the study to the first harmonic of the response, so  $p = 1$ . In this case, the amplitude of the response is given by

$$\widehat{X} = \sqrt{A_1^2 + B_1^2} \quad (16)$$

For the case of the mechanical system subjected to random vibrations,  $p$  is chosen to be equal to the number of samples  $N$  in connection with the frequency resolution  $\Delta f$ . More explanations will be given in Section 5.1 on the choice of  $N$  for the mechanical system under study.

Equation (11) can be rewritten in the Fourier basis:

$$KB_0 = C_0 \quad (17)$$

$$\begin{bmatrix} K_{lin} - (k\Omega)^2 M & -k\Omega C_{lin} \\ k\Omega C_{lin} & K_{lin} - (k\Omega)^2 M \end{bmatrix} \begin{bmatrix} A_k \\ B_k \end{bmatrix} = \begin{bmatrix} S_k \\ C_k \end{bmatrix} + \begin{bmatrix} S_{k,excit} \\ C_{k,excit} \end{bmatrix} \quad \forall k \in [1;p] \quad (18)$$

The coefficients  $C_0$  and  $(S_k, C_k)_{k \in [1;p]}$  depend on the coefficients  $B_0$  and  $(A_k, B_k)_{k \in [1;p]}$ . They are calculated through an adaptation of the classical Alternate Frequency Time domain method (AFT-method) [18]. The following process is proposed and implemented

$$\mathbf{X} = [B_0, A_1, B_1, \dots, A_p, B_p] \xrightarrow{FFT^{-1}} X(t) \xrightarrow{HilbertFiltering} \widehat{X} \xrightarrow{Eq. (12)} F_{nl}(t) \xrightarrow{FFT} \mathbf{B}_{NL} = [C_0, S_1, C_1, \dots, S_p, C_p] \quad (19)$$

Let's start from  $B_0$  and  $(A_k, B_k)_{k \in [1;p]}$ , the harmonic components of the response. The calculation of the amplitude of  $X(t)$  for each  $t$  is performed by using an inverse FFT procedure. In the general case, the amplitude of  $X(t)$  over time cannot be defined properly, but in many cases,  $X(t)$  is a narrow-band signal, typical of the response of a single degree-of-freedom system. In this case, the amplitude of excitation is slowly evolving over time and a filtering technique can follow the evolution of the amplitude. Figure 7 shows a narrow-band signal (blue) and the estimation of its amplitude with two different filterings (i.e. a Hilbert analytical filtering [19] in red, and a second order Butterworth filtering [20] in green). In this example it appears that the Butterworth filter presents a lag compared to the Hilbert signal. The main difference in the two filters is that the Hilbert signal requires the complete temporal signal in order to be computed. With the HBM, the AFT method requires calculating the temporal signal  $X(t)$  completely, so the Hilbert method can be used. In this work a Hilbert filtering for the HBM method is implemented. Then the calculation of the nonlinear force  $F_{nl}(t)$  can be performed based on the approximation of  $\widehat{X}$ . Finally, using a FFT procedure, the harmonic components  $C_0$  and  $(S_k, C_k)_{k \in [1;p]}$  of the nonlinear force in the frequency-domain are estimated.

It can be noted that the process defined in Equation can be simpler in the case of swept-sine experiments where the response  $X(t)$  is necessarily a sine, since  $p = 1$ . In this case, the amplitude of  $X(t)$  is known from Equation (16), and there is no need to use the AFT. The process is then written in the form

$$\mathbf{X} = [B_0, A_1, B_1, \dots, A_p, B_p] \xrightarrow{Eq. (16)} \widehat{X} \xrightarrow{Eq. (12)} \mathbf{B}_{NL} = [C_0, S_1, C_1, \dots, S_p, C_p] \quad (20)$$

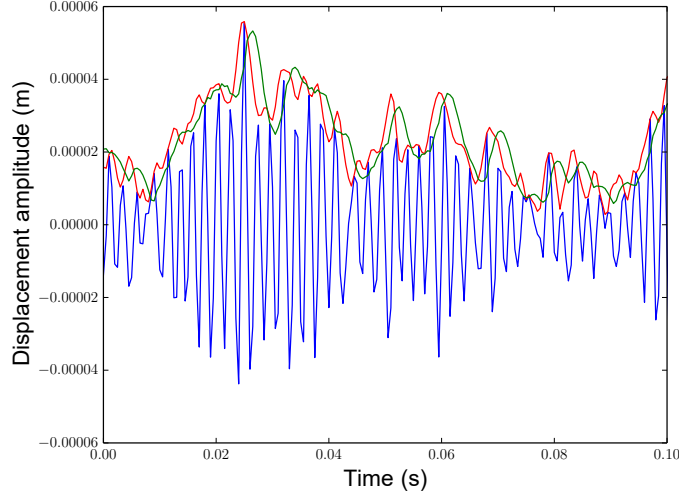


Figure 7: Narrow-band temporal signal (blue) and its envelope through a Butterworth filtering (green) and a Hilbert filtering (red)

This link between  $C_0$ ,  $(S_k, C_k)_{k \in [1;p]}$  and  $\mathbf{X}$  enables a nonlinear solving of the nonlinear problem (Equations 17 and 18) which can be written as  $\mathbf{H}(\mathbf{X}, \Omega, F) = \mathbf{0}$ .

Finally the nonlinear problem is solved using a continuation procedure with a predictor-corrector scheme [17] in order to obtain a continuous response curve in the frequency domain. For the case of the mechanical system subjected to swept-sine excitations: a Newton-Raphson continuation method is used by considering the frequency  $\Omega$  and the Fourier coefficients  $\mathbf{X}$  as variables. For the mechanical system subjected to random excitations, the solution  $\mathbf{X}$  of  $\mathbf{H}(\mathbf{X}, \Omega, F) = \mathbf{0}$  corresponds to the Fourier transform of the stationary solution over the entire frequency band. This solution  $\mathbf{X}$  can thus be used to estimate the PSD of the solution. So there is no need to use a continuation procedure with a predictor-corrector scheme. However, problems of convergence can appear at high levels of excitation. Therefore it can be interesting to use a continuation procedure by considering the input PSD of the random excitation and the Fourier coefficients  $\mathbf{X}$  as variables. This continuation process starts at low levels of excitation (when the non-linearity is not excited) to the required excitation level. This procedure allows a better convergence of the nonlinear solution for high level of random excitations. More details can be found in [12].

#### 4.2. Shooting method

The shooting method allows the periodic solution of the mechanical system to be estimated without making assumptions regarding its form, as opposed to the HBM method.

Considering the equations of motion (11) in state space form (with  $\mathbf{Z} = [X, \dot{X}]^T$ ), we have

$$\dot{\mathbf{Z}} = \mathbf{G}(\mathbf{Z}, t) \quad (21)$$

where

$$\mathbf{G}(\mathbf{Z}, t) = \left[ \dot{X}, \frac{1}{M} \left( -K_{lin}X - C_{lin}\dot{X} + F_{nl}(\hat{X}) + F(t) \right) \right]^T \quad (22)$$

Considering the process of temporal integration, a difficulty emerges: for a time  $t$ , all the terms of the equation are known, but in order to go to the next time increment, one needs to know the value of  $\hat{X}$ . To do so, a second order Butterworth filter is introduced:

$$\ddot{\hat{Y}} + 2\omega_f\mu_f\dot{\hat{Y}} + \omega_f^2\hat{Y} = \omega_f^2X^2 \quad (23)$$

with  $\omega_f$  and  $\mu_f$  the pulsation and the damping of the filter, respectively. In practice, the following values has been chosen for the present study:  $\omega_f = \frac{1}{3}\omega_0$  and  $\mu_f = 0.5$ . Adding the filtering equation to Equation (22), it becomes

$$\mathbf{G}(\mathbf{Z}, t) = \left[ \dot{X}, \frac{1}{M} \left( -K_{lin}X - C_{lin}\dot{X} + F_{nl}(\hat{X}) + F(t) \right), \dot{\hat{Y}}, -\omega_f^2\hat{Y} - 2\omega_f\mu_f\dot{\hat{Y}} + \omega_f^2X^2 \right]^T \quad (24)$$

with  $\mathbf{Z} = [X, \dot{X}, \hat{Y}, \dot{\hat{Y}}]^T$ . Following the resolution of the problem giving access to quantities  $X$  and  $\hat{Y}$ , the variable  $\hat{X}$  can be directly calculated by  $\hat{X} = \sqrt{2\hat{Y}}$ .

For the swept-sine experiments, the input signal  $F(t)$  is periodic with one fundamental harmonic of pulsation  $\omega$ . For random inputs, the signal has been modeled by a sum of periodic signals (see Section 3), so the function  $F(t)$  is also periodic such that the associated period  $T$  is equal  $\frac{1}{\Delta f}$  with  $\Delta f$  the frequency resolution of the random input. The solution of system (21) with the initial condition  $\mathbf{Z}(t=0) = \mathbf{Z}_0$  is written as  $\mathbf{Z}(t, \mathbf{Z}_0)$  in order to exhibit the dependency on the initial conditions. Such a solution is stationary if it is periodic of minimal period  $T = \frac{1}{\Delta f}$ .

The shooting algorithm solves numerically the two-point boundary-value problem (i.e. the initial condition  $\mathbf{Z}(t, \mathbf{Z}_0)$  and a solution  $\mathbf{Z}(T, \mathbf{Z}_0)$  in order to find the initial condition  $\mathbf{Z}_0$  that verifies the condition of periodicity given by

$$\mathbf{H}(\mathbf{Z}_0, T) = \mathbf{Z}(T, \mathbf{Z}_0) - \mathbf{Z}_0 = 0 \quad (25)$$

The determination of  $\mathbf{Z}(T, \mathbf{Z}_0)$  is performed by a time-integration method on a discrete time basis of the interval  $[0, T]$ . A fourth order Runge-Kutta integration scheme with an adaptive calculation step control is used.

## 5. Numerical results and comparisons with experiments

In this section, experiments and numerical simulations with harmonic or random experimental inputs are compared. Firstly, a brief discussion of the signal parameters used in numerical simulations is presented. Secondly comparisons between experiments and numerical results are undertaken for both harmonic and random excitations. More specifically analysis of the results based on swept-sine tests is performed in order to validate and to discuss the limitations of the proposed modeling of elastomer. The comparisons between simulations and experiments for random excitations are undertaken in order to demonstrate the efficiency of the proposed modeling strategy and the associated numerical methodology.

### 5.1. Updating of the signal parameters in the case of random excitations

First of all, updating of the signal parameters previously discussed in Section 3.3.2 has to be performed in regard to the case under study. The nonlinear vibration of the rubber isolator subjected to random excitations will be calculated in the bandwidth of interest [50;600] Hz. So the Nyquist frequency imposes that the time step is  $dt = \frac{1}{2 \times 600} = 8.33 \cdot 10^{-4}$  s or less.

Considering the frequency resolution, one must be able to properly capture the resonance peak of the mechanical structure ‘‘Unitarian Gamma Joint’’. A common and classical choice is to have 8 points in the mid-power interval of the resonance peak which corresponds to a resolution  $\Delta f$  given by

$$\Delta f = f_0 \left( 1 - \sqrt{1 - 2\xi \tan\left(\frac{\pi}{16}\right)} \right) \quad (26)$$

where  $f_0$  is the frequency of the resonance peak and  $\xi$  defines the associated damping ratio damping (i.e.  $\xi = \frac{1}{2Q}$  with  $Q$  the quality factor). Having extremely low  $\Delta f$  is problematic because it is then necessary to have many harmonics for a given bandwidth, which will impact the computational time of the simulations. The lowest  $\Delta f$  would be obtained for very high quality factors  $Q$  and very low frequency. In the case under study, the quality factor  $Q$  decreases with frequency because of the Payne effect. The worst case scenario is obtained for the maximum value of the quality factor  $Q$  that is measured experimentally for the lowest excitation level (i.e.  $Q = 15$ ) and the lowest resonance frequency that is measured experimentally for the highest excitation level (i.e.  $f_0=200$  Hz). This leads to a resolution  $\Delta f = 1.5$  Hz. Considering a Nyquist frequency  $f_n = 1200$  Hz, this leads to

a minimum number of samples  $N = \frac{f_n}{\Delta f} = 800$ . Conventionally, the number of samples  $N$  is taken as a power of 2 to simplify the use of the FFT, so the number of samples  $N$  is chosen equal to  $2^{10} = 1024$  for the numerical simulations. Consequently the total time  $T$  of the signal is given by  $T = (N - 1) \times dt = 0.85$  s.

### 5.2. Harmonic excitations - validation and limitations of the elastomer modeling

The prediction of the nonlinear vibrations of the rubber isolator subjected to sinusoidal excitations is compared with the swept-sine experiments previously presented in Section 2.2. Figure 8 shows the comparisons of numerical results and experiments for five excitation levels ( $1 \text{ m s}^{-2}$ ,  $5 \text{ m s}^{-2}$ ,  $10 \text{ m s}^{-2}$ ,  $40 \text{ m s}^{-2}$  and  $120 \text{ m s}^{-2}$ ). For each simulation, the input corresponds to the fundamental of the experimental input previously discussed and shown in Section 2.2. In Figure 8, simulation results are presented for both the HBM and the shooting simulations. The relative difference between results from the two methods are less than 1% and therefore not really visible on the nonlinear response of the elastomer. It can be reminded that the use of a Butterworth filtering signal may introduce a lag to compute the amplitude of displacement, which should be translated into a discrepancy in the response. This undesirable phenomena is not visible in the present case due to the fact that the amplitude of displacement is constant over time for sinusoidal signals. The Butterworth filtering technique therefore gives a perfect approximation of the amplitude of displacement.

As expected, the peak resonance, as well as the softening effect are perfectly predicted for the different excitation levels. It can be concluded that all these results validate the modeling of elastomer developed in Section 3.1. Nevertheless, a discrepancy appears between simulations and experiments for the high excitation levels ( $40 \text{ m s}^{-2}$  and  $120 \text{ m s}^{-2}$ ). This difference is more particularly visible for the frequency band located after the resonance peak and this difference between experiments and simulations seems to increase with the level of excitation (see for example Figure 8 for the three excitation levels  $10 \text{ m s}^{-2}$ ,  $40 \text{ m s}^{-2}$  and  $120 \text{ m s}^{-2}$ ). The phenomenon can be explained physically by considering the fact that an increase in temperature for high excitation levels is observed during experiments. More specifically this reflects the heating of the elastomeric material during an experimental test and a strong temperature dependency of the mechanical properties of the elastomer. So this small discrepancy between experiments and numerical results after the resonance peaks for high excitation levels is due to the relative simplicity of the proposed modeling of the elastomer which does not take into account thermal effects.

Nonetheless, the modeling of the elastomer is good enough to capture the resonance peak, the softening effect as well as the general form of the nonlinear response after the resonance peak for all excitation levels. The discrepancies between the simulations and the experiments are small enough to conclude on the validity of the simplified modeling and the identification methodology of the associated parameters.

### 5.3. Random vibrations

Now the prediction of the nonlinear vibrations of the rubber isolator subjected to random excitation is compared with the experiments previously presented in Section 2.2. Results are given in Figure 9 for four excitation levels ( $1 \text{ m s}^{-2}$  RMS,  $20 \text{ m s}^{-2}$  RMS,  $40 \text{ m s}^{-2}$  RMS and  $80 \text{ m s}^{-2}$  RMS). For each simulation, the input corresponds to the PSD of the experimental input previously discussed in Section 2.2. The peak resonance, as well as the softening effect and the global nonlinear behavior are perfectly predicted for all the random excitations. Moreover comparisons between experiments and simulations are also very satisfactory for the prediction of the nonlinear responses on the whole bandwidth of interest whatever the nonlinear method used. This validates without any ambiguity the modeling of elastomer, as well as the modeling of the random signal and the proposed nonlinear methodology developed in Section 4.

In contrast to the results for the harmonic excitations, a relative difference between the simulation results from the HBM and the shooting method is visible on the nonlinear response of the rubber isolator, even if the predictions proposed for each method are very good compared to the experimental tests. This difference on the numerical results of the two methods comes from the filtering techniques

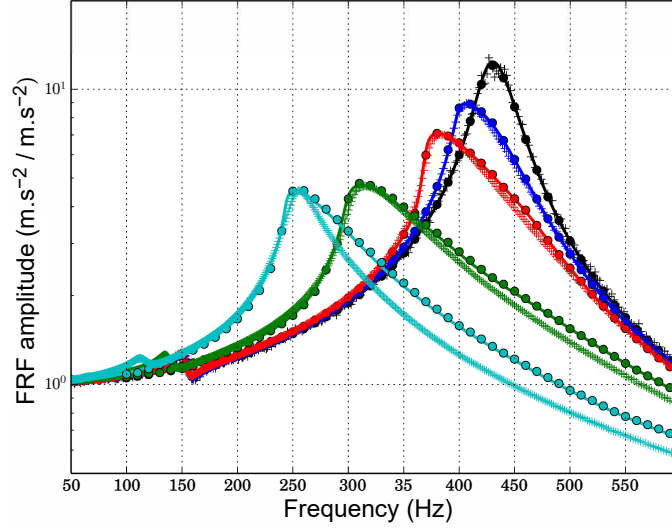


Figure 8: Experimental FRFs for swept-sine experiments (crosses) with HBM simulations (lines) and shooting simulations (dots) for the excitation levels  $1 \text{ m s}^{-2}$  (black),  $5 \text{ m s}^{-2}$  (blue),  $10 \text{ m s}^{-2}$  (red),  $40 \text{ m s}^{-2}$  (green) and  $120 \text{ m s}^{-2}$  (cyan)

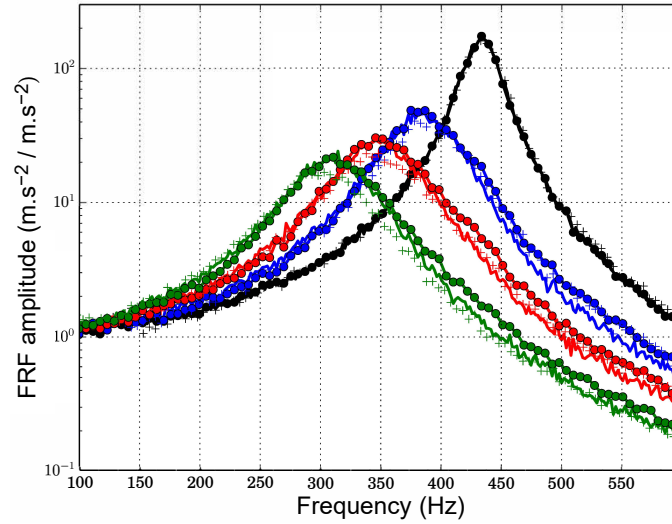


Figure 9: Experimental random FRFs (crosses) with HBM simulations (lines) and shooting simulations (dots) for the excitation levels  $1 \text{ m s}^{-2}$  RMS (black),  $20 \text{ m s}^{-2}$  RMS (blue),  $40 \text{ m s}^{-2}$  RMS (red) and  $80 \text{ m s}^{-2}$  RMS (green)

employed for the HBM (i.e. filtering) and for the shooting method (i.e. Butterworth filtering). For more details the interested reader is referred to [12].

Furthermore, it can be noted that the temperature effect is less visible for random vibrations than for swept-sine experiments (see and compare Figures 8 and 9 for high excitation levels)/ This can be easily explained by the fact that for experimental tests with random excitations the elastomer temperature remains constant during the experiment, while it varies greatly during swept-sine experiments. This validates the choice of the simplified elastomeric modeling for the rubber isolator subjected to random excitations.

Even if this simplified modeling appears to be sufficient for all the present study, the fact that the temperature has an impact (even if it is very weak) for sine-swept experiments whereas no effect is visible for random excitation, demonstrates the difficulty of proposing an adequate or advanced modeling in practice for engineering problems. Indeed the nonlinear vibration response strongly depends on the operating conditions (i.e the swept-sine experiments or random excitations in the present study) that induces physical phenomena which are not always easily controlled (i.e. the elastomer temperature in the present study). All the difficulty is to be able to decide on whether to consider or not the inclusion of these physical phenomena (i.e. the temperature in the present case) to propose advanced modeling allowing a perfect prediction of the nonlinear response. Taking

into account such phenomena requires the establishment of an experimental protocol that not only allows to identify the additional parameters needed for the modeling but also to be able to estimate the evolution of these added parameters versus operating conditions during experiments. Thus it is sometimes preferable to remain on simplified but mastered and controlled models that are sufficient to reproduce in a very satisfactory way the non-linear effects observed and the global vibrational behavior of the mechanical system under study.

## 6. Conclusions and future work

This paper deals with the experimental and numerical study of a rubber isolator subjected to both harmonic and random excitations. First of all, nonlinear phenomena are observed experimentally. The dependency of the dynamical properties on the elastomeric material with respects to the excitation level, the temperature and the load history is observed. A simple modeling of elastomer that makes the hypothesis that the Payne effect is dominant over the other nonlinear contributions is developed. This model of the rubber isolator is adapted to complex nonlinear simulations, including responses to harmonic and random excitations.

The prediction of the nonlinear vibration of the beam subjected to swep-sine or random excitations is performed by using an adaptation of the HBM or shooting method. The comparisons between tests and simulations for sine-swept experiments and random excitations demonstrate the relevance of the global method and the validity of the retained elastomeric model that is simple yet sufficient. The correlations are perfect for low excitation levels on the entire frequency range. For the higher excitation levels, the resonance peak and the associated amplitudes as well as the softening effect are well predicted. The tendencies of the evolution of the vibratory levels after the resonance peak follow the experimental tendencies, with a small shift for sine-swept experiments. This shift is mainly due to a heating of the elastomeric compound caused by high excitations.

## Acknowledgment

J.-J. Sinou acknowledges the support of the Institut Universitaire de France.

## References

- [1] J. Harris, A. Stevenson, On the role of nonlinearity in the dynamic behavior of rubber components, *Rubber Chemistry and Technology* 59 (5) (1986) 740–764.
- [2] M. Sjöberg, L. Kari, Testing of nonlinear interaction effects of sinusoidal and noise excitation on rubber isolator stiffness, *Polymer Testing* 22 (3) (2003) 343 – 351.
- [3] R. Lewandowski, B. Chorazyczewski, Identification of the parameters of the kelvin-voigt and the maxwell fractional models, used to modeling of viscoelastic dampers, *Computers and Structures* 88 (1) (2010) 1 – 17.
- [4] M. M. Sjöberg, L. Kari, Non-linear behavior of a rubber isolator system using fractional derivatives, *Vehicle System Dynamics* 37 (3) (2002) 217–236.
- [5] M. Berg, A non-linear rubber spring model for rail vehicle dynamics analysis, *Vehicle System Dynamics* 30 (3-4) (1998) 197–212.
- [6] N. Gil-Negrete, J. Vinolas, L. Kari, A simplified methodology to predict the dynamic stiffness of carbon-black filled rubber isolators using a finite element code, *Journal of Sound and vibration* 296 (4-5) (2006) 757–776.
- [7] V. Jaumouillé, J.-J. Sinou, B. Petitjean, Simulation of payne effect of elastomeric isolators with a harmonic balance method, *Shock and Vibration* 19 (6) (2012) 1281–1295.
- [8] C. Xueqian, S. Zhanpeng, H. Qinshu, D. Qiang, L. Xin'en, Influence of uncertainty and excitation amplitude on the vibration characteristics of rubber isolators, *Journal of Sound and Vibration* 377 (2016) 216–225.
- [9] D.-W. Sun, Z.-G. Chen, G.-Y. Zhang, P. Eberhard, Modeling and parameter identification of amplitude-and frequency-dependent rubber isolator, *Journal of Central South University of Technology* 18 (3) (2011) 672.
- [10] M. Claeys, J.-J. Sinou, J.-P. Lambelin, B. Alcoverro, Multi-harmonic measurements and numerical simulations of nonlinear vibrations of a beam with non-ideal boundary conditions, *Communications in Nonlinear Science and Numerical Simulation* 19 (12) (2014) 4196–4212.
- [11] M. Claeys, J.-J. Sinou, J.-P. Lambelin, R. Todeschini, Experiments and numerical simulations of nonlinear vibration responses of an assembly with friction joints–application on a test structure named “harmony”, *Mechanical Systems and Signal Processing* 70 (2016) 1097–1116.

- [12] T. Roncen, J. Lambelin, J.-J. Sinou, Nonlinear vibrations of a beam with non-ideal boundary conditions and stochastic excitations - experiments, modeling and simulations, *Communications in Nonlinear Science and Numerical Simulation* 74 (2019) 14–79.
- [13] N. Hansen, A. Ostermeier, Completely derandomized self-adaptation in evolution strategies, *Evolutionary computation* 9 (2) (2001) 159–195.
- [14] M. Shinozuka, Simulation of multivariate and multidimensional random processes, *The Journal of the Acoustical Society of America* 49 (1B) (1971) 357–368.
- [15] M. Shinozuka, C.-M. Jan, Digital simulation of random processes and its applications, *Journal of sound and vibration* 25 (1) (1972) 111–128.
- [16] W. H. Press, S. Teukolsky, W. Vetterling, B. Flannery, *Numerical Recipes in Fortran 77*, Press Syndicate of the University of Cambridge, 1996.
- [17] E. Sarrouy, J.-J. Sinou, *Non-linear periodic and quasi-periodic vibrations in mechanical systems – on the use of the harmonic balance methods*, INTECH Open Access Publisher, 2011.
- [18] T. Cameron, J. Griffin, An alternating frequency time domain method for calculating the steady state response of nonlinear dynamic systems, *Journal of Applied Mechanics* 56 (1989) 149–154.
- [19] S. L. Hahn, *Hilbert transforms in signal processing*, Artech House, 1996.
- [20] I. W. Selesnick, C. S. Burrus, Generalized digital butterworth filter design, *IEEE Transactions on signal processing* 46 (6) (1998) 1688–1694.